



Pergamon

Available online at www.sciencedirect.com

SCIENCE @ DIRECT®



www.actamat-journals.com

Acta Materialia 51 (2003) 1261–1270

Short-range ordering and $\{1,1/2,0\}$ diffuse intensity maxima in ZrN_x

P. Li *, J.M. Howe

Department of Materials Science and Engineering, University of Virginia, 116 Engineers Way, Charlottesville, VA 22904-4745, USA

Received 21 August 2002; received in revised form 21 August 2002; accepted 25 October 2002

Abstract

Diffuse intensity maxima in ZrN_x caused by short-range ordering (SRO) of nitrogen atoms or vacancies are shown in electron diffraction patterns along four different low-index zone-axes. Analysis of the shape of the diffuse intensity was performed using an equation developed by Sauvage and Parthé [1]. Additional $\{1,1/2,0\}$ diffuse intensity maxima were also observed and these have not been previously reported for interstitial carbides and nitrides with a NaCl-type crystal structure. Both a Kohn construction, which assumes that the positions of $2k_{F110}$ yield the diffuse intensity maxima, and microdomain crystal models based on M_2X or M_4X_3 crystal structures, are presented as possible explanations for the origin of the $\{1,1/2,0\}$ diffuse intensity maxima. The close relationship between the SRO model and the shape of the Fermi surface indicates that the Fermi surface in ZrN has nearly the same shape as that of TiN .

© 2003 Acta Materialia Inc. Published by Elsevier Science Ltd. All rights reserved.

Keywords: Transmission electron microscopy; Short-range ordering; Vacancies; ZrN

1. Introduction

When a compound has many point defects but an insufficient concentration to produce long-range ordering (LRO), short-range ordering (SRO) may occur. This causes diffraction effects that give diffuse intensity maxima in reciprocal space. A clear example of this phenomenon occurs in the transition-metal carbides such as TiC , VC and NbC [2,3]. In nitrides, evidence for diffuse intensity has

been found in TiN , but not in VN [2]. Such diffuse intensity features are normally ascribed to SRO of vacancies or interstitial atoms [1,4]. Diffuse intensity maxima and SRO have not been reported for ZrN , which has the same NaCl crystal-structure type as the carbides and nitrides above.

A geometrical model proposed by Sauvage and Parthé [1] successfully explains the shape of diffuse intensity surfaces in ordered transition-metal carbides and nitrides. However, the diffuse intensity is not always uniform and was found to have maxima at the $\{1,1/2,0\}$ positions in $(Ti,Mo)C_x$ [4]. This diffuse intensity was produced by a short-range body-centered tetragonal, ordered structure of the Ti_4Mo type [4,5]. The $\{1,1/2,0\}$ diffuse

* Corresponding author. Tel.: +1-434-9825659; fax: +1-434-9825660.

E-mail address: p13k@virginia.edu (P. Li).

intensity has not been observed in other transition-metal carbides and nitrides with a NaCl crystal structure containing only two elements.

The $\{1,1/2,0\}$ diffuse maxima also occur in alloys such as Ni-rich Ni–Mo, Ni–V [6], and Au–Cr [7]. The maxima are due to stacking of the $\{420\}$ planes in microdomains of different tetragonal lattices such as $D0_{22}$, $D1_a$, and Pt_2Mo . Theoretical analysis also indicates that A_2B_2 crystal structures can produce $\{1,1/2,0\}$ diffuse intensity maxima, although no such A_2B_2 alloys are known to exist [8,9]. Since SRO tends to have a pre-configuration of the RO state [10], it may be possible to build a crystallographic model to explain the origin of SRO in ZrN if one understands the crystal structures of the possible LRO phases in transition-metal carbides and nitrides with NaCl crystal-structure type.

A different approach to explain diffuse scattering maxima has been developed using the Krivoglaž–Clapp–Moss (KCM) theory [9,11–13]. This theory relates the Fourier transform of the effective pair interaction (EPI) energy parameters $V(k)$ to the SRO scattering and usually, the diffuse intensity has a maximum where $V(k)$ is minimum. Based on this theory, a Kohn construction was used to explain the fourfold splitting of the diffuse scattering about the $\{110\}$ positions in Cu_3Au alloy [14]. The same procedure could be used for ZrN if information about the Fermi surface and k vector were available. Such information can be obtained from experimental data that reveal the diffuse intensity surface. Sauvage and Parthé [1] have found a close relationship between the diffuse intensity model and the Fermi surface model, indicating that diffuse scattering also can be used to obtain information about the Fermi surface of compounds. Construction of the Fermi surface from the shape of the diffuse intensity has been also performed for titanium oxide, where good agreement was obtained [15].

The present paper describes diffuse intensity maxima and SRO in ZrN_x . The origin of SRO is also investigated using *in situ* electron irradiation. Both the KCM theory and crystallographic models are used to explain the observed diffuse intensity maxima. Discussion of the Fermi surface of ZrN is also provided.

2. Specimen preparation and experimental procedures

2.1. Sample preparation

The ZrN sample used in this study was prepared by encapsulating a 50 μm -thick foil of high-purity α -Zr in a sealed quartz tube under an atmosphere of high-purity N and annealing for 2 h at 1200 °C. The N content of the foil was determined to be 31.9 at% from the increase in weight of the nitrated specimen compared with the initial high-purity Zr foil. To produce a homogeneous distribution of N throughout the foil and to obtain a two-phase mixture of α -Zr + ZrN, the nitrated foil was annealed for 10 h at 1200 °C in an encapsulated tube filled with high-purity Ar and then quenched into cold water. Regions of ZrN in the two-phase specimen were selected for transmission electron microscopy (TEM) observation.

Disks 3 mm in diameter were cut from the foil using an ultrasonic cutter. Three different thinning methods were employed in order to prepare thin foils of the brittle nitrated samples: (1) A double-jet technique was used to electrolytically thin the disks. An electrolyte of perchloric acid and methanol in the ratio 3:97 by volume was used, and the disk specimens were thinned in this electrolyte at 18 V and at -50 °C. Final thinning was obtained by cold-stage ion-beam milling for 1 h. (2) The 3 mm diameter disk was glued on a Cu grid using epoxy glue and then dimpled to 20 μm thickness. Final thinning was performed by ion-beam milling at 5 kV for 6 h. (3) A tripod polisher was used to thin the 3 mm disks on both sides to achieve a thickness of 15 μm . Final thinning was performed by ion-beam milling for 4 h.

2.2. TEM procedures

The thinned specimens were examined in a JEOL 2000FXII electron microscope operating at 200 kV. Electron diffraction patterns, each of which provides a two-dimensional slice of the intensity distribution in reciprocal space, were obtained for many different specimen orientations using a large-angle tilting stage. These two-dimensional sections were combined to establish the

three-dimensional distribution of the diffuse intensity in reciprocal space. Long exposure times, such as 90–180 s, were used to reveal the weak diffuse intensity in the patterns. *In situ* electron irradiation experiments on ZrN were also performed in the 2000FXII microscope at room temperature. The beam current-density used during irradiation was approximately 0.2 A/cm².

3. Results

3.1. Diffuse intensity maxima and SRO in ZrN

Fig. 1 clearly shows diffuse intensity maxima in the [001], [011], [111] and [112] zone-axes in ZrN, confirming that SRO is present. The shapes of the diffuse intensity maxima are the same as those

observed in transition-metal carbides [2,3] and have been analyzed theoretically by Sauvage and Parthé [1]. These investigators assumed that the value of the diffuse intensity is constant along a given surface and zero elsewhere. They proposed a geometric model for the diffuse intensity distribution using the following equation [1]:

$$\cos(\pi h) + \cos(\pi k) + \cos(\pi l) \quad (1)$$

$$+ 3C \cos(\pi h) \cos(\pi k) \cos(\pi l) = 0,$$

where the empirical parameter C , which ranges from -1 to 0 , describes the shape variation of the diffuse intensity surface. The pattern of diffuse intensity calculated for the four different zone-axes in Fig. 1, according to Eq. (1), are shown in Fig. 2. The results shown by dashed lines in Fig. 2 correspond to $C = 0$ and those shown by full lines correspond to $C = -1$.

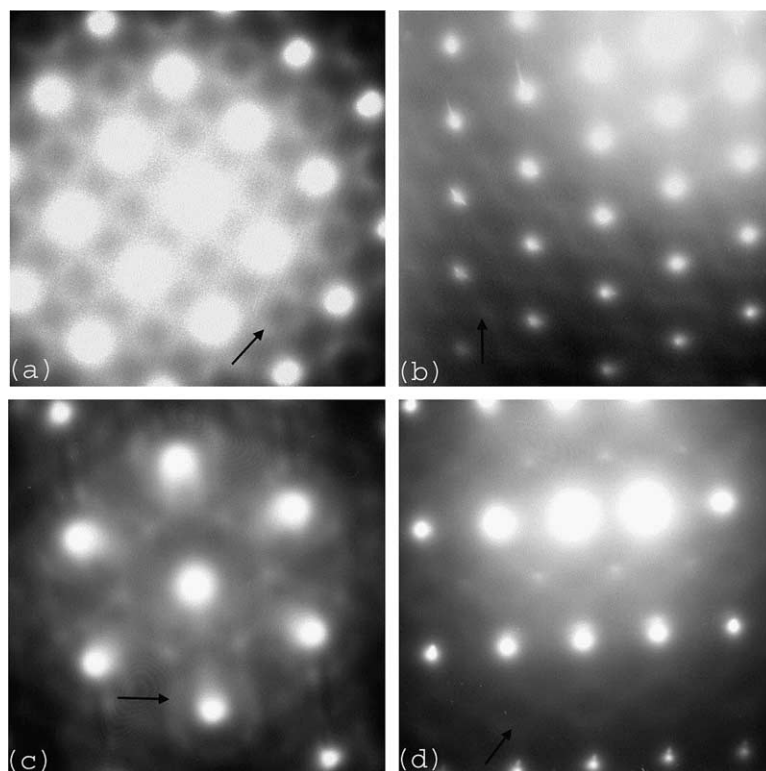


Fig. 1. Diffuse intensity due to SRO of vacancies in electron diffraction patterns from ZrN observed along four different zone-axes: (a) [001], (b) [011], (c) [111], and (d) [112]. Arrows indicate the positions of intensity maxima.

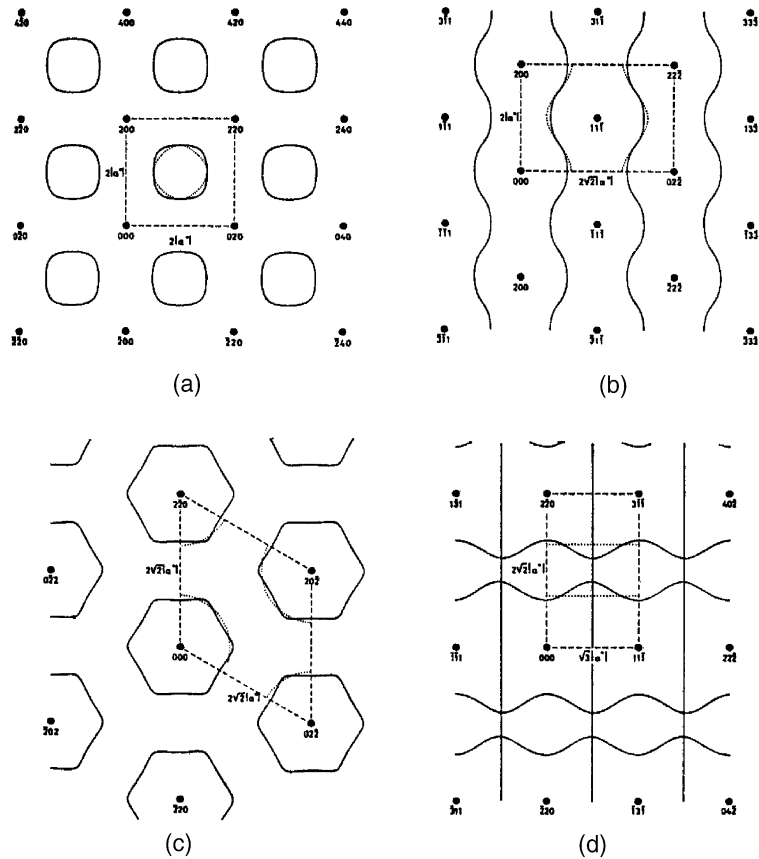


Fig. 2. Calculated diffuse intensities for transition-metal carbides and nitrides along different zone-axes [1]: (a) [001], (b) [011], (c) [111], and (d) [112]. Dashed lines correspond to $C = 0$ and full lines to $C = -1$.

The parameter C can be determined by the following equation [1]:

$$C = -\frac{1 + 2 \cos 2\pi F}{3 \cos^2 2\pi F} \quad (2)$$

$$\text{with } F = \frac{1}{2} \frac{D_{(000-220)} - D_{\text{diff}}}{D_{(000-220)}}$$

where $D_{(000-220)}$ is the spacing between the 000 and 220 diffraction spots and D_{diff} is the distance between the two diffuse bands. Thus, C can be obtained by measuring $D_{(000-220)}$ and D_{diff} in Fig. 1(a)–(c). These measurements show that D_{diff} is approximately 0.35 of $D_{(000-220)}$, which in turn gives a value of $C = -0.15$. This value is close to that of TiN [1]. The shape of the diffuse inten-

sity tends to be circular in Fig. 1(a) rather than square, which is in good agreement with the calculated results shown for $C = 0$ in Fig. 2.

While there is good agreement between the general shape of the diffuse intensity in Figs. 1 and 2, there is a significant increase in the diffuse intensity at the $\{1,1/2,0\}$ positions in ZrN in Fig. 1(a) that is not present in the calculations in Fig. 2. Similar diffuse intensities have been reported in $(\text{Ti,Mo})\text{C}_x$ and these were explained by Ti_4Mo metal-atom ordering [4,5], but this is different from ZrN because there is only one metallic element in this phase. Further investigation of the origin of SRO was performed by *in situ* electron irradiation of ZrN in the TEM, as described in the next section.

Fig. 3. Electron diffraction patterns from ZrN as a function of 200 kV electron irradiation in the TEM: (a) before irradiation, (b) irradiated for 600 s, and (c) irradiated for 3000 s. Note the disappearance of the diffuse intensity, such as that indicated by an arrow in (a), with increasing irradiation.

3.2. *In situ* electron irradiation of ZrN

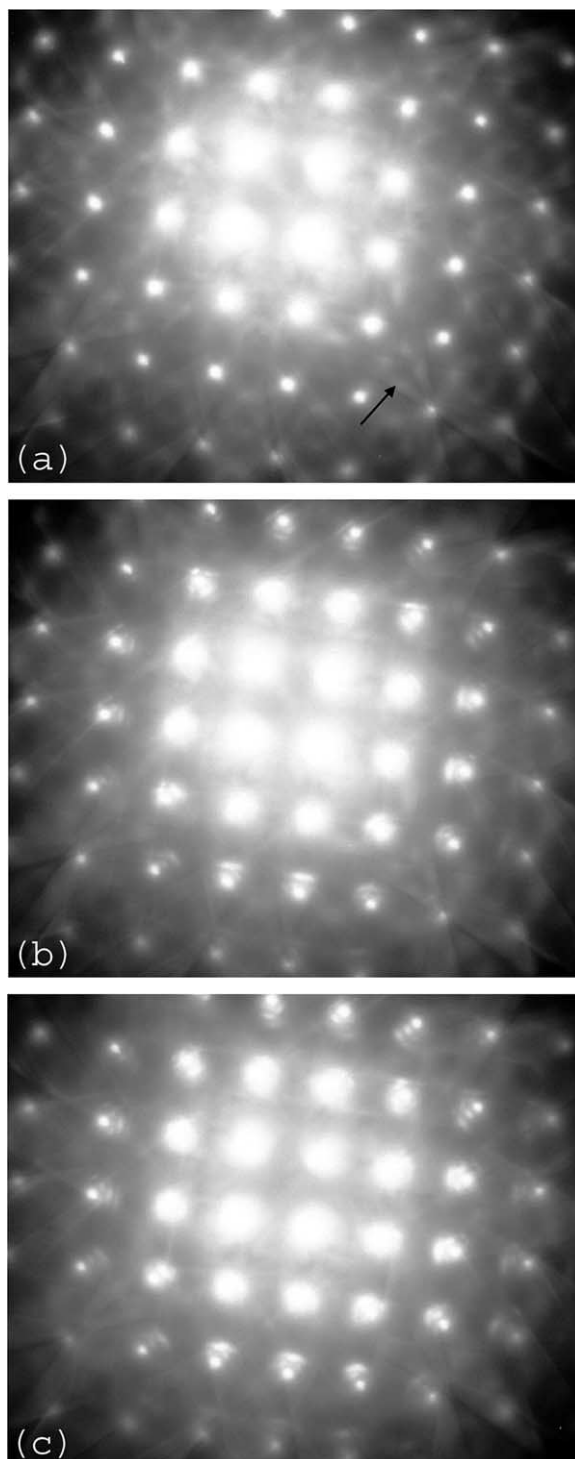
In situ electron irradiation experiments were performed in the JEOL2000FXII microscope to determine whether or not the SRO observed in the ZrN phase is due to nitrogen-vacancy ordering. The results of these experiments are shown in Fig. 3. Clear diffuse intensity maxima at the $\{1,1/2,0\}$ position are evident in the diffraction pattern in Fig. 3(a), which was taken immediately before exposure to the electron beam. The diffuse intensity became weaker after the specimen was irradiated for 600 s at 200 kV in the TEM, as shown in Fig. 3(b). Finally, the diffuse intensity disappeared in Fig. 3(c), after further irradiation at 200 kV for 3000 s.

The disordering evident in Fig. 3 is not due to thermal effects from the 200 kV electron beam. The thermal conductivity of ZrN is approximately 20.5 W/m K, which means that ZrN is a good thermal conductor [16]. Beam heating is generally negligible in metals and other good conductors under standard TEM conditions, because the temperature change is only a few degrees centigrade [17].

An explanation for the disordering effect seen in Fig. 3 can be attributed to collision between the 200 kV electrons and N atoms in ZrN. The maximum energy transferred to the target atoms in an electron–atom collision E_p , is given by the following equation [5,18]:

$$E_p = \frac{2E(E + 2mc^2)}{Mc^2}, \quad (3)$$

where c is the velocity of light, E the energy of the incident electrons, and m and M are the masses of the electron and target atom, respectively. The displacement of an atom occurs when $E_p > E_d$, where E_d is the threshold energy for atom displacement. The threshold energy E_d for the displacement of C atoms in monocarbides was estimated as about 5 eV, whereas the energy for the metal atoms was estimated as 20–40 eV [5]. Although values



of E_d for N and Zr are not available, it is reasonable to assume that the value of E_d for N is nearly the same as that of C, because the masses and bonding in these two atoms are similar. It is also reasonable to assume that E_d for Zr atoms is 20–40 eV, which is typical for many metal atoms. Substituting the electron mass, and the mass values for N and Zr into Eq. (3) above, one finds that E_p for N is 17.2 eV and E_p for Zr is 5.7 eV, under 200 keV electron irradiation. The value of E_p is much greater than the threshold value of E_d for N, which means that displacement of N atoms occurs under 200 keV electron irradiation. The situation is reversed for Zr atoms. Thus, 200 kV electron irradiation provides sufficient energy to knock N atoms off their interstitial sites, scrambling their SRO arrangement with vacancies, which are also present on these sites. This results in the loss of diffuse intensity maxima at the $\{1,1/2,0\}$ positions (Fig. 3) and explains the origin of the diffusive intensity in ZrN.

4. Discussion

4.1. Possible fermi surface in ZrN

As mentioned previously in Section 1, the shape of the diffuse intensity in transition-metal carbides and nitrides is strikingly similar to the shape of the theoretical Fermi surface of a primitive cubic metal, so that the diffuse scattering can be used to obtain information about the Fermi surfaces in these compounds. Castles et al. [15] have performed such analyses for titanium oxide, where a close relationship between the shape of the diffuse intensity and the Fermi surface was obtained. By comparing the calculated shapes of the Fermi surfaces for TiC and TiN [19] shown in Fig. 4 with the diffuse intensity in the $[001]$ (Fig. 1(a)) and $[011]$ (Fig. 1(b)) zone-axes of ZrN, it is evident that the experimental data for the projection of the diffuse intensities conform well to the (001) and (011) sections of the Fermi surfaces for TiN (Fig. 4(b)), but not to those of TiC (Fig. 4(a)). These results suggest that the Fermi surface of ZrN is more like that of TiN [19–21] than TiC [19,20].

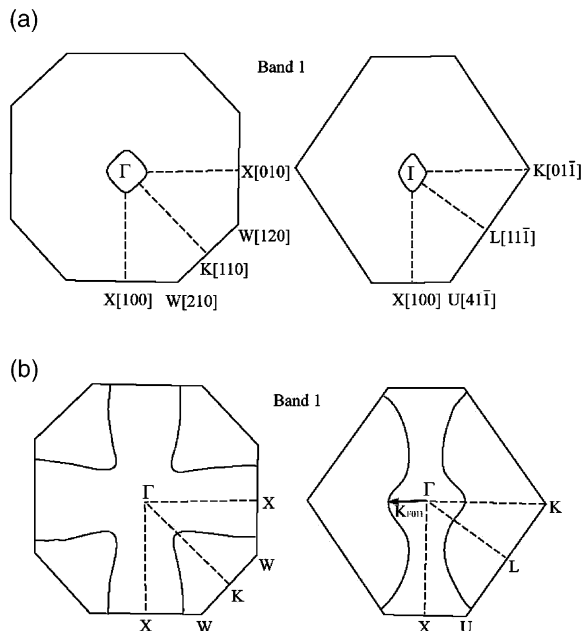


Fig. 4. Calculated Fermi surface sections in the first Brillouin zone of: (a) TiC, and (b) TiN [19].

4.2. KCM explanation for the origin of $\{1,1/2,0\}$ diffuse intensity in ZrN

It is currently possible to perform ab initio electronic structure calculations in order to understand the structure and stability of phases. A generalized Ising Hamiltonian (H) is often used to describe the energy of formation of a binary A–B alloy [10–14]. The ordering energy ΔE_{ord} derived from H , that describes the difference between the actual state and a statistically uncorrelated arrangement, is given by:

$$\Delta E_{\text{ord}} = NC^A C^B \sum_{lmn \neq 000} V_{lmn} \alpha_{lmn}, \quad (4)$$

where N is the number of the lattice sites. C^A and C^B are the atomic fractions of A and B atoms, which satisfy the identity: $C^A + C^B = 1$. α_{lmn} are the Warren–Cowley short-range order parameters, which relate to the occupation of atomic sites separated by a lattice vector, given by:

$$\alpha_{lmn} = 1 - \frac{P_{lmn}^{AB}}{C^B} = 1 - \frac{P_{lmn}^{BA}}{C^A}, \quad (5)$$

where P_{lmn}^{AB} is the conditional probability that given an atom A at the origin of space there is a B atom in the neighboring shell lmn of an A–B alloy. V_{lmn} are the EPI energy parameters, given by:

$$V_{lmn} = \frac{V_{lmn}^{AA} + V_{lmn}^{BB} - 2V_{lmn}^{AB}}{2}, \quad (6)$$

where V_{lmn}^{AA} , V_{lmn}^{BB} and V_{lmn}^{AB} are the various nearest-neighbor bond energies. Based on this theory, the KCM approximation directly relates the Fourier transform of the EPI energy parameters $V(k) = \sum_{lmn} V_{lmn} e^{ikr_{lmn}}$ to the short-range order scattering in Laue units, $I_{SRO}(k)$, as [9,11,12]:

$$I_{SRO}(k) = \frac{D}{1 + 2C^A C^B V(k)/k_B T} \quad (7)$$

where k_B is Boltzmann’s constant, T is temperature and with the normalization factor D close to 1.

Eq. (7) indicates that maxima in the diffuse intensity occur at positions in reciprocal space with a minimum value of $V(k)$. As was first indicated by Roth et al. [22], parallel flat sections of the Fermi surface can give rise to a log singularity in $V(k)$ at $2k_F$, where $2k_F$ is the distance between the flats. Such singularities appear as minima in $V(k)$ and should be observable as traces of those pieces of Fermi surface that are responsible for them. This theory was able to successfully explain the fourfold splitting of diffuse scattering about the $\{110\}$ positions in Cu_3Au alloy using a Kohn construction [14]. We use the same procedure below, to explain diffuse intensity maxima at the $\{1,1/2,0\}$ positions in ZrN .

According to the calculations for SRO in Fig. 2(b)–(d), the shape of the projected diffuse intensity indicated by dashed lines indicates that there is a tendency to have flatness normal to the $\langle 110 \rangle$ directions. This means that we can use $2k_{F110}$ to make a Kohn construction in a (001) reciprocal lattice section for ZrN . Fig. 5(a) shows this construction to illustrate the $\{1,1/2,0\}$ diffuse intensity maxima that occur in ZrN . The value of k_{F110} ($k_{F110} = k_{F011}$ by symmetry) was obtained from the experimental data in Fig. 1(b), shown enlarged in Fig. 5(b). When two ‘anomalous’ $2k_F$ surfaces cross, an approximate doubling of the depth of the minimum in $V(k)$ occurs, giving rise to a doubling

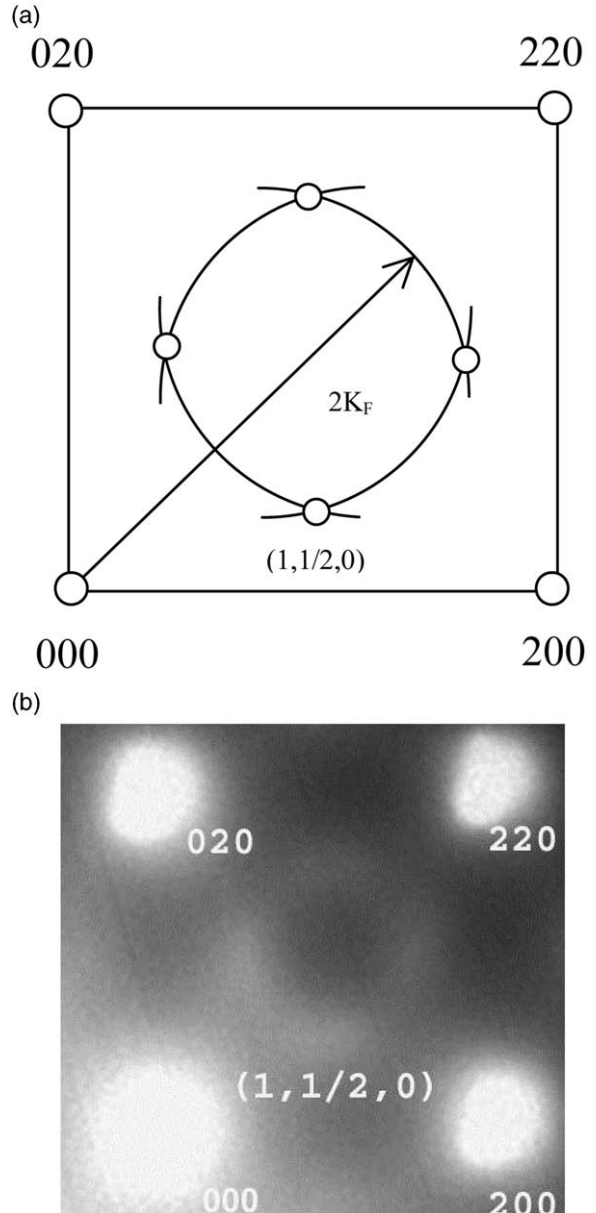


Fig. 5. (a) Kohn construction for the (001) plane in ZrN , using $2k_{F110}$ centered about the four fundamental diffraction spot positions, and (b) experimental data for ZrN , shown enlarged from Fig. 1.

of intensity near the $\{1,1/2,0\}$ positions shown in Fig. 5(b).

4.3. Crystallographic explanation for the origin of $\{1,1/2,0\}$ diffuse intensity in ZrN

Successful explanation of the diffuse intensity in reciprocal space based on the Fermi surface construction lead us to further consider whether or not we could explain this phenomenon in real space. Okamoto and Thomas [6] have previously explained the close relationship between stable/metastable ordered structures in alloys such as Ni-rich Ni–Mo and Ni–V, both of which display $\{1,1/2,0\}$ diffuse intensity maxima in the SRO state. These crystal structures can be constructed by consecutive stacking of $\{420\}$ planes to yield different ordered arrangements, such as the $D0_{22}$ structure (stacking sequence AAAB...), the $D1_a$ structure (AAAAB...), and the Pt_2Mo -type structure (AAB...). Based on high-resolution TEM results, Van Tendeloo and Amelinckx [7] interpreted the $\{1,1/2,0\}$ SRO in Au_4Cr and Ni_4Mo as being due to the presence of microdomains of $D0_{22}$ structure with elements of the $D1_a$ structure, that sometimes extend several unit cells along the c -direction, while being only one or a small number of unit cells wide. Theoretical analysis [8,9] has also shown that it is possible to have an A_2B_2 alloy, which consist of $\{420\}$ planes with an AAB... stacking sequence that give rise to $\{1,1/2,0\}$ diffuse maxima, although no such A_2B_2 alloys are known to exist. It is known that SRO can be expected to represent something like a pre-configuration of the LRO state, and this makes it possible to investigate whether or not the same type of $\{420\}$ planar stacking and crystal structures discussed above might apply for ZrN.

Unfortunately, few experimental results concerning possible LRO phases in Zr–N alloys have been published. Two possible metastable phases were recently identified: one was Zr_4N with a monoclinic crystal structure by Sharma et al. [23,24] and another was tentatively identified as Zr_2N with a tetrahedral body-centered crystal structure by Li and Howe [25]. The details of these LRO phases are not presented here as the purpose of this discussion is to emphasize that only a few LRO phases have been identified and many unknown phases are likely to exist in this system.

Computational research on LRO in interstitial

compounds, especially in the systems Ti–C, Zr–C and Ti–N, has been performed by Gusev and Rempel [26–28]. From this work, two ordered phases with the tetragonal crystal structures shown in Fig. 6 are important, because the A_2B_2 , $D0_{22}$, $D1_a$ and Pt_2Mo structures, which can display $\{1,1/2,0\}$ diffuse intensity maxima, all have a tetragonal lattice. The superstructure shown in Fig. 6(a) is a tetragonal M_2X -type structure (space group $I4_1/amd$) and the Ti_2N phase with this structure has been identified in the Ti–N system [29,30]. Fig. 6(b) shows a tetragonal M_4X_3 superstructure (space group $I4/mmm$). An ordered phase with this structure has not been previously found in interstitial carbides and nitrides, but it appears that such a phase could form in the Zr–N system, as discussed subsequently.

The two superstructures in Fig. 6 can be considered as two tetragonal interpenetrating sublattices, one containing metal atoms (M) and the other containing interstitial atoms (N) and vacancies (V). If we ignore the metal atom sublattice, the remaining tetragonal sublattices containing interstitial atoms and vacancies are shown in Fig. 7. It is important to note that Fig. 7(a) yields an A_2B_2 crystal structure with an AAB... stacking sequence of $\{420\}$ planes. Fig. 7(b) yields a $D0_{22}$ crystal structure with an AAAB... stacking sequence of $\{420\}$ planes if one considers that the A planes contain vacancies and the B planes consist of interstitial atoms. These two crystal structure models are able to predict the origin of $\{1,1/2,0\}$

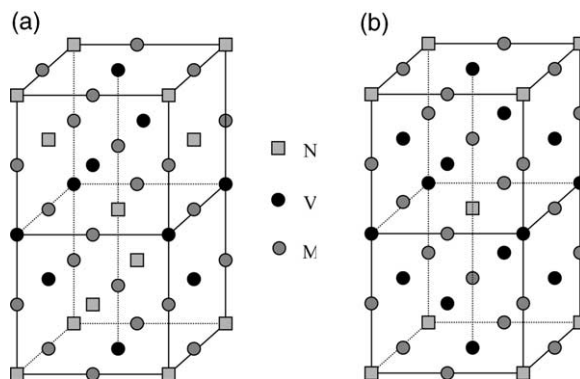


Fig. 6. (a) M_2X and (b) M_4X_3 crystal structure types with N occupying the X positions.

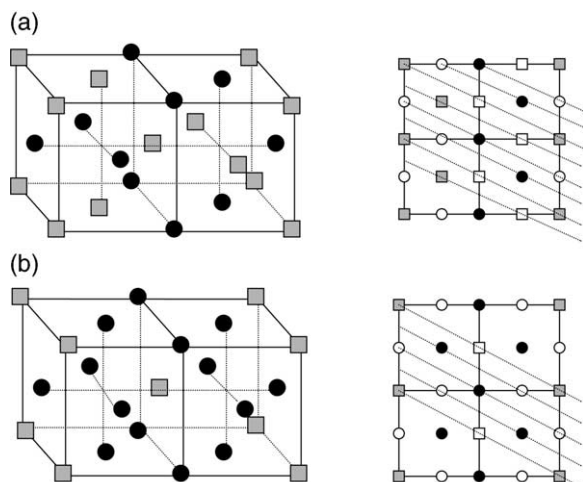


Fig. 7. The A_2B_2 and A_3B ($D0_{22}$) crystal structures showing various $\{420\}$ planes indicated by dotted lines in the right figures occupied by vacancies (A planes) or N atoms (B planes): (a) A_2B_2 with an AAB... stacking of the $\{420\}$ planes, and (b) A_3B with a BAAAB... stacking of the $\{420\}$ planes.

diffuse maxima in ZrN as due to SRO ordering of vacancies and N atoms along the $\{420\}$ planes. This provides a crystallographic basis for the origin of the $\{1,1/2,0\}$ diffuse intensity maxima in ZrN. Thus, both the Fermi surface analysis and simultaneous ordering of N and vacancies are able to provide different approaches to understand the appearance of diffuse intensity maxima in electron diffraction patterns from the ZrN phase. Further confirmation of these explanations and the physical connection between the two analyses may come from future work on LRO phases in the Zr–N system.

The crystallographic models of SRO in ZrN are different from those used for FCC alloys in the past. Thus, it is likely that $\{1,1/2,0\}$ diffuse intensity might occur in other interstitial alloys with M_2X and M_4X_3 -type tetragonal crystal structures. The only difference is that the diffuse intensity in these superstructures should be weaker than that in the $D0_{22}$, $D1_a$ and Pt_2Mo structures, due to the dominant role of the metal sublattice atoms on the diffraction pattern intensities. This means that it will be more difficult to detect $\{1,1/2,0\}$ diffuse intensity maxima in interstitial alloys with M_2X and M_4X_3 tetragonal crystal structures.

5. Conclusions

Electron diffraction patterns displaying prominent diffuse intensity were observed along four different low-index zone-axes in ZrN. Such diffuse intensity comes from the SRO of vacancies and N atoms, which was confirmed by in situ electron irradiation experiments, which destroyed this ordered arrangement at room temperature. Additional $\{1,1/2,0\}$ diffuse intensity maxima were also observed in ZrN and these have not been previously reported for interstitial carbides and nitrides with a NaCl-type crystal structure. Analysis of the shape of the diffuse intensity was performed using an equation developed by Sauvage and Parthé [1]. The close relationship between the SRO model and the shape of the Fermi surface leads us to conclude that the Fermi surface in ZrN has nearly the same shape as that of TiN. A Kohn construction was used to explain the $\{1,1/2,0\}$ diffuse intensity maxima, assuming that the position of $2k_{F110}$ yields the diffuse intensity maxima. Microdomain crystal models were also presented to explain the origin of the $\{1,1/2,0\}$ diffuse intensity maxima. These models consist of either an A_2B_2 superstructure with an AAB... stacking sequence of the $\{420\}$ planes, or a $D0_{22}$ superstructure with an AAAB... stacking sequence of the $\{420\}$ planes, or both, where A represents planes of vacancies and B represents planes of interstitial atoms. Confirmation of these models may be achieved by future discovery of new metastable LRO phases in the Zr–N system. From a crystallographic viewpoint, we conclude that $\{1,1/2,0\}$ diffuse intensity maxima can be observed in alloys with M_2X or M_4X_3 crystal structures, which are different from the $D0_{22}$, $D1_a$ and Pt_2Mo -type structures, where this effect has been observed previously.

Acknowledgements

This research was supported by the National Science Foundation under grant DMR-9908855. The authors also thank Prof G.C. Weatherly for his help with the ZrN system and Profs. W.A. Jesser and G.J. Shiflet for use of their encapsulating equipment.

References

- [1] Sauvage M, Parthé E. Acta Cryst. A 1972;A28:607.
- [2] Billingham J, Bell PS, Lewis MH. Acta Cryst. A 1972;A28:602.
- [3] Buršík J, Weatherly GC. Phys Status Solidi A 1999;174:327.
- [4] Murata Y, Yukawa N. J. Less-Common Metals 1988;141:235.
- [5] Murata Y, Yukawa N. J. Less-Common Metals 1988;141:309.
- [6] Okamoto PR, Thomas G. Acta Metall. 1971;19:825.
- [7] Van Tendeloo G, Amelinckx S. Acta Cryst. B 1985;B41:281.
- [8] Fontaine DD. Acta Metall. 1975;23:553.
- [9] Clapp PC, Moss SC. Phys. Rev. 1968;171:754.
- [10] Schönfeld B. Prog. Mater. Sci. 1999;44:435.
- [11] Clapp PC, Moss SC. Phys. Rev. 1966;142:418.
- [12] Moss SC, Clapp PC. Phys. Rev. 1968;171:764.
- [13] Krivoglaz MA. Diffuse scattering of X-rays and neutrons by fluctuations. Berlin: Springer, 1996.
- [14] Moss SC. Phys. Rev. Lett. 1968;22:1108.
- [15] Castles JR, Cowley JM, Spargo AEC. Acta Cryst. A 1971;A27:376.
- [16] Pierson H. Handbook of refractory carbides and nitrides. New Jersey: Noyes Publications, 1996.
- [17] Williams DB, Carter CB. Transmission electron microscopy. New York: Plenum Press, 1996.
- [18] Seitz F, Koehler JS. In: Seitz F, Turnbull D, editors. Solid state physics, vol. 2. New York: Academic Press; 1956.
- [19] Ern V, Switendick AC. Phys. Rev. 1965;137(6A):1927.
- [20] Schadler G, Weinberger P. Solid State Commun. 1984;51(1):35.
- [21] Winzer K, Reichelt J. Solid State Commun. 1984;49(5):527.
- [22] Roth ML, Zeiger HJ, Kaplan TA. Phys. Rev. 1966;149:519.
- [23] Sharma S. MS thesis, University of Virginia; 2001.
- [24] Sharma S, Howe JM. Philos Mag A, in press.
- [25] Li P, Howe JM. Unpublished research, University of Virginia; 2002.
- [26] Gusev AI. Phys. Status Solidi B 1991;163:17.
- [27] Gusev AI, Rempel AA. Phys. Status Solidi A 1993;135:15.
- [28] Gusev AI, Rempel AA. Phys. Status Solidi A 1997;163:273.
- [29] Christensen AN, Alamo A, Landesman JP. Acta Cryst. C 1985;C41:1009.
- [30] Nagakura S, Kusunoki T. J. Appl. Crystallogr. 1977;10:52.